Title

The effect of core—shell engineering on the energy product of magnetic nanometals

Journal

Chemical Communications, 54(78)

ISSN

1359-7345

Authors

Zhang, Wei

Yang, Weibing

Chandrasena, Ravini U

et al.

Publication Date

2018-09-27

DOI

10.1039/c8cc05978k

Peer reviewed

ChemComm

COMMUNICATION

View Article Online
View Journal | View Issue

Cite this: *Chem. Commun.*, 2018, **54**, 11005

Received 24th July 2018,
Accepted 6th September 2018

DOI: 10.1039/c8cc05978k

rsc.li/chemcomm

The effect of core–shell engineering on the energy product of magnetic nanometals†

Wei Zhang,[a] Weibing Yang,[b] Ravini U. Chandrasena,[b] V. Burak Özdöl,[c] Jim Ciston,[c] Michael Kornecki,[d] SelvaVennila Raju,[d] Raymond Brennan,[d] Alexander X. Gray[b] and Shenqiang Ren *[a]

Solution-based growth of magnetic FePt–FeCo (core–shell) nanoparticles with a controllable shell thickness has been demonstrated. The transition from spin canting to exchange coupling of FePt–FeCo core–shell nanostructures leads to a 28% increase in the coercivity (12.8 KOe) and a two-fold enhancement in the energy product (9.11 MGOe).

Over the past few decades, magnetic nanoparticles have made significant contributions to modern technology, gaining interest for use in data storage materials, magnetic resonance imaging devices, and power generation systems.[1] However, with the growing concern over energy efficiency and environmental impact, earth-abundant magnetic materials with enhanced energy products are urgently needed. The rational design and growth of magnetic nanocomposites comprising two or more materials has been considered a promising strategy to enhance the energy product of magnets.[2–9] In this context, magnetic core–shell nanocomposites that couple magnetically hard and soft phases could simultaneously achieve high magnetocrystalline anisotropy and saturation magnetization.[6–12] These core–shell architectures could enable the magnetic properties (such as the thermal stability of magnetization and coercivity) to be efficiently tuned *via* the control of the core–shell parameters, including the shape, size, and chemical composition.[13–16] It has been shown that magnetic $CoFe_2O_4$–$MnFe_2O_4$ core–shell nanoparticles with interfacial spin interactions can be beyond the theoretical limit of their energy product.[17] There is an immediate need for simple, scalable and reliable synthesis methods for manufacturing high-performance metallic core–shell nanocomposites with coupling interactions between the core and shell interfaces.

Here, a solution-based technique for the preparation of FePt–FeCo (core–shell) nanostructures with controlled shell thickness is demonstrated. An interface coupling (spin canting) effect is evident in the FePt–FeCo nanoparticles when the average thickness of the as-grown FeCo shell is 0.9 ± 0.279 nm. The resulting core–shell FePt–FeCo nanoparticles indicate a substantial enhancement in magnetic coercivity (12.8 KOe), and a two-fold increase in the energy product (9.11 MGOe) at room temperature, compared to the FePt nanoparticles.

Fig. 1a illustrates the schematic growth of FePt nanostructures with different morphologies. The FePt nanoparticles with average diameters of 2.8 ± 0.183 nm were synthesized using dioctyl ether as the reaction solvent (Fig. 1b). When switching the reaction solvent from dioctyl ether to oleyamine, the nanowire morphology is dominant in the as-synthesized FePt (Fig. S1, ESI†).[18] A variety of stoichiometric FePt nanoparticles with the chemical composition of $Fe_{18}Pt_{82}$, $Fe_{42}Pt_{58}$, and $Fe_{61}Pt_{39}$ were synthesized by controlling the reaction conditions (Fig. S2, ESI†). It should be noted that the composition of the as-synthesized Fe_xPt_{100-x} had an influential effect on the size of the resultant particles after sintering (Fig. 1d).[19] By increasing the amount of Pt (Fe) during the sintering process, the extra Pt (Fe) atoms could be substitutionally placed on the $L1_0$ Fe (Pt) sublattice, effectively transforming the structure to a cubic phase with a reduced magnetocrystalline anisotropy.[20] Therefore, a lower phase transition temperature and increased particle growth could be demonstrated in either the sintered Pt-rich ($Fe_{18}Pt_{82}$; average particle size of 400 nm) or Fe-rich ($Fe_{61}Pt_{39}$; average particle size of 10 μm) particles,[21] while the stoichiometric $Fe_{42}Pt_{58}$ nanoparticles could withstand higher sintering temperatures prior to the agglomeration, leading to a smaller particle size (the average diameter of 50 nm). The stoichiometry of FePt nanoparticles could also play a vital role in defining magnetic properties. As shown in Fig. 1e, the as-synthesized $Fe_{42}Pt_{58}$ nanoparticles exhibit a coercivity (H_c) of 4500 Oe, a remanent

[a] *Department of Mechanical and Aerospace Engineering, and Research and Education in Energy, Environment & Water (RENEW) Institute, University at Buffalo, The State University of New York, Buffalo, NY 14260, USA. E-mail: shenren@buffalo.edu*
[b] *Department of Physics, Temple University, Philadelphia, Pennsylvania 19122, USA*
[c] *National Center for Electron Microscopy Facility, Molecular Foundry, Lawrence Berkeley National Laboratory, Berkeley, California 94720, USA*
[d] *U.S. Army Research Laboratory, Aberdeen Proving Ground, Maryland 21005, USA*

† Electronic supplementary information (ESI) available: Sample preparation and additional structural characterization. See DOI: 10.1039/c8cc05978k

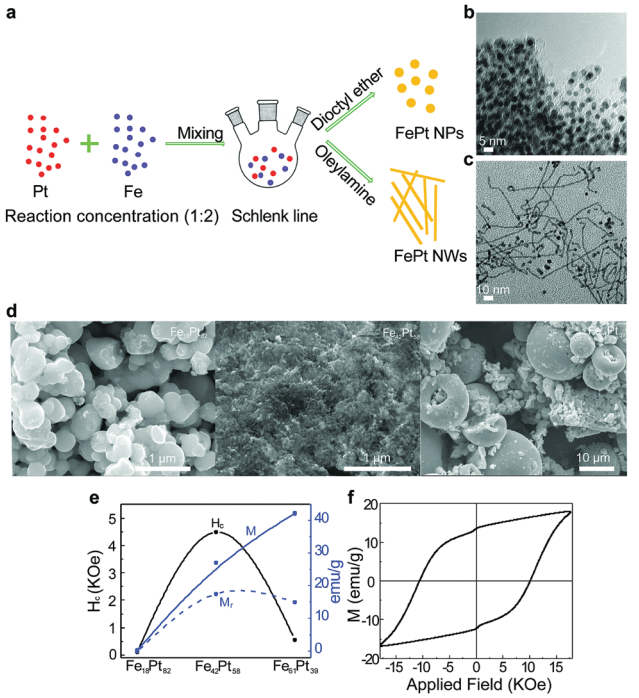

Fig. 1 Solution growth of FePt nanostructures. (a) Schematic process of FePt nanoparticles and nanowire growth, showing the importance of reaction solvents for morphological control. (b and c) Transmission electron microscopy (TEM) images of as-synthesized FePt nanoparticles and nanowires. (d) Scanning electron microscopy (SEM) images of FePt nanoparticles with different elemental ratios ($Fe_{18}Pt_{82}$, $Fe_{42}Pt_{58}$, and $Fe_{61}Pt_{39}$) after sintering at 773 K for 2 h. (e) Element ratio-dependent coercivity (H_c), remanent magnetization (M_r) and saturation magnetization (M_s) of FePt nanoparticles after sintering at 773 K for 2 h. (f) The magnetic hysteresis loop of $Fe_{42}Pt_{58}$ nanoparticles after sintering at 1023 K for 2 h at room temperature.

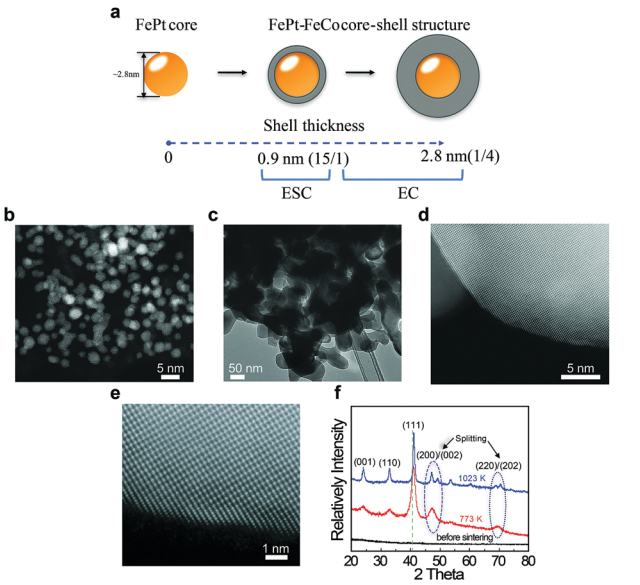

Fig. 2 Growth of FePt–FeCo core–shell nanoparticles. (a) Schematic illustrations for the synthesis of FePt–FeCo core–shell nanoparticles with a tunable shell thickness (0.9–2.8 nm). (b) TEM image of FePt–FeCo nanoparticles before sintering. (c) Low magnification TEM images of FePt–FeCo samples after sintering at 1023 K for 2 h. (d and e) High-resolution STEM images of annealed FePt–FeCo core–shell structures with the lattice ordering loss at the last ~1 nm of surface shell. (f) XRD patterns of the as-synthesized FePt–FeCo before and after sintering at 773 K and 1023 K, respectively. The peak splitting indicates the phase transition from fcc to $L1_0$ FePt.

magnetization (M_r) of 17.5 emu g^{-1}, and a saturation magnetization (M_s) of 27 emu g^{-1}. In contrast, the Fe-rich $Fe_{61}Pt_{39}$ nanoparticles exhibit a larger saturation magnetization (M_s, 43 emu g^{-1}) and a much smaller coercivity (H_c, 510 Oe), while the Pt-rich $Fe_{18}Pt_{82}$ nanoparticles demonstrate the lowest magnetic properties (M_s of 0.4 emu g^{-1} and H_c of 101 Oe). After sintering, the coercivity of $Fe_{42}Pt_{58}$ nanoparticles could be increased to 10 KOe with a decrease in saturation magnetization (Fig. 1f), suggesting a face-centered cubic (fcc) conversion to the $L1_0$–FePt structure confirmed by XRD.

For magnetic alloys, strongly enhanced properties could be realized by coupling magnetically hard and soft phases that simultaneously achieve high magnetocrystalline anisotropy and high saturation magnetization. By varying the FeCo shell thickness, FePt–FeCo core–shell nanocrystals could be synthesized with properties close to their optimal values. For this reason, the as-synthesized FePt nanoparticles were mixed with Fe and Co precursors at 433 K, leading to the growth of FeCo shells. Fig. 2a shows the schematic representation of the shell thickness control in FePt–FeCo core–shell nanoparticles. The average FeCo shell thickness was adjusted from 0.9 ± 0.279 nm to 2.8 ± 0.827 nm at a constant stoichiometry of $Fe_{42}Pt_{58}$ by increasing the precursor concentration (Fig. 2a and Fig. S3, ESI†). The details for the synthetic control are shown in the ESI† section. It should be noted that the reaction temperature was lower than the temperature required for FeCo particle formation, as the pre-formed FePt cores served as nuclei from which the deposition of FeCo shells originated.

Fig. 2b shows a TEM image of the FePt–FeCo core–shell nanoparticles before sintering, with an average shell thicknesses of 0.9 ± 0.279 nm and homogeneous particle size distributions. The chemical compositions, containing constituent Fe, Pt and Co elements, were confirmed *via* energy dispersive X-ray spectroscopy (EDS, Fig. S4, ESI†). After sintering at 1023 K, the particles exhibited a heterogeneous distribution, with sizes ranging from 5 nm to 200 nm, as shown in Fig. 2c–e. High-resolution scanning TEM images of FePt–FeCo in Fig. 2d provide the explicit microstructural details of the sample with clear lattice fringes, confirming the high crystallinity of the annealed FePt–FeCo. Furthermore, a ~1 nm surface layer that lost the FePt $L1_0$ ordering confirmed that an fcc-FeCo shell was formed (Fig. 2e),[22] which was consistent with the XRD results (the standard ICDD data 00-026-1139, Fig. 2f). The XRD spectra were further collected to investigate the effect of different sintering temperatures on phase evolution in the FePt–FeCo structures (Fig. 2f). Before sintering, no discernable diffraction peaks (black spectrum) were observed for the as-synthesized FePt–FeCo nanoparticles.[23,24] After sintering at 773 K (red spectrum), a series of diffraction peaks could be resolved, with the strong peaks corresponding to the (111) plane at 40.3° and the (200) plane at 47.2°, representing fcc-FePt nanostructures. After sintering at 1023 K (blue spectrum),

the broad peaks became sharper, and more importantly, new shoulder peaks appeared at 49° and 71°, corresponding to the (002) and (202) planes, respectively. The splitting of the peaks at 47.2° and 69.8° suggested phase transformation of FePt from fcc to $L1_0$,[25] indicating the formation of $L1_0$ FePt at 1023 K. In addition, a (111) peak shift (the green dash line in Fig. 2f) was observed when compared with the standard ICDD data (00-026-1139), suggesting the existence of the FeCo shell. The related lattice distortion could be responsible for the enhanced energy product.

The correlation between the FeCo shell thickness and magnetic properties of FePt–FeCo was examined by measuring field-dependent magnetization. As shown in Fig. 3a, the FePt–FeCo particles exhibited smooth magnetic hysteresis curves with insignificant variations, implying well-coupled core–shell phases. The FePt-only core had an H_c value of 10 kOe and a saturation magnetization (M_s) of 17 emu g^{-1} (black dashed line). As the average thickness of the FeCo shell increased (2.1 ± 0.148 nm, 2.4 ± 0.436 nm, 2.8 ± 0.827 nm), the FePt–FeCo core–shell structures showed a corresponding increase in M_s from 88 to 104 emu g^{-1}.[26] In contrast, the H_c values exhibited a hyperbolic decrease when compared to the pure FePt sample. The thick (2.8 ± 0.827 nm) FeCo shell exhibited an H_c value of 487 Oe. The changes in H_c and M_s served as examples of exchange coupling (EC) behavior between magnetically hard FePt cores and soft FeCo shells. However, as the shell thickness decreased (1.2 ± 0.374 nm, 1.1 ± 0.089 nm, and 0.9 ± 0.279 nm), the FePt–FeCo nanoparticles exhibited an unusual phenomenon, with significantly increased H_c values to 8.2 KOe, 8.7 KOe, and 12.8 KOe, respectively. For the thin (0.9 ± 0.279 nm) FeCo shells, the H_c values of the FePt–FeCo nanostructures were 30% higher than that of the FePt cores. Meanwhile, the decrease in M_s of FePt–FeCo nanostructures was relatively small, from 37 to 32 emu g^{-1}, but larger than that of the FePt cores. Fig. 3b shows the relationship between M_s and H_c for FePt–FeCo nanostructures with different shell thicknesses. Unlike the typical core–shell nanoparticles in the EC regime (*i.e.* FePt–FeCo with a shell thickness larger than 2 nm), the thin-shelled FePt–FeCo nanoparticles possessed larger anisotropic energy barriers as compared to the FePt core materials, which was representative of an enhanced spin canting effect (ESC) as opposed to exchange coupling.[17,27] When the shell thickness was similar in size to the crystalline unit-cell (1 nm), the population of canted spins located at the interface between FePt cores and FeCo shells increased, requiring a larger external magnetic field to neutralize it. This was consistent with the enhanced H_c value,[17,27] which could be attributed to the interfacial ESC effect.

The sintering temperature played an essential role in achieving phase transition of the magnetic FePt–FeCo nanostructures, leading to an investigation of these temperature effects on the magnetic properties of FePt–FeCo. As shown in Fig. 3c, the FePt–FeCo nanoparticles, with the shell thicknesses of 0.9 ± 0.279 nm, exhibit largely enhanced H_c values from 2.1 kOe to 12.8 kOe for the sintering temperature from 773 K to 1023 K, respectively. The relationship between M_s and H_c for FePt–FeCo (1.2 ± 0.374 nm, 1.1 ± 0.089 nm, and 0.9 ± 0.279 nm) was plotted as a function of sintering temperature (Fig. 3d). When compared to the change in M_s, a much larger increase in H_c was observed, indicating that the sintering temperature plays a significant role in the phase transition of FePt from fcc to $L1_0$. Meanwhile, the slight decrease in M_s could be attributed to the diffusion of FeCo into the FePt core. The results indicated that the shell thickness played an important role in determining the magnetic properties of FePt–FeCo nanoparticles. The magnetic phenomenon in the ESC regime of the as-prepared core–shell composites could potentially be utilized for the development of high-performance nanomagnets.

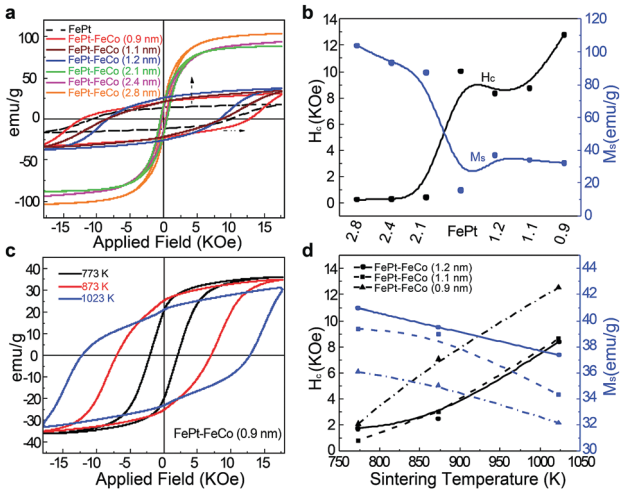

Fig. 3 Magnetic properties of FePt–FeCo core–shell nanoparticles. (a) Magnetic hysteresis loops of FePt nanoparticles with various shell thicknesses measured at room temperature. (b) Shell thickness-dependent H_c and M_s curves of FePt–FeCo nanoparticles. (c) Sintering temperature-dependent magnetic hysteresis loops for FePt–FeCo nanoparticles with an average thickness of 0.9 nm. (d) Variation of H_c and M_s as a function of sintering temperature for FePt–FeCo with different shell thicknesses.

The controlled thickness of the FeCo shell onto the FePt core enabled tunability of the energy product $(BH)_{max}$ evolution in FePt–FeCo nanostructures. Fig. 4a illustrates the B–H curves of sintered FePt cores, as well as a series of FePt–FeCo nanostructures with different shell thicknesses. As shown in Fig. 4b, the measured $(BH)_{max}$ for the FePt core is 3.54 MGOe. The $(BH)_{max}$ value increased to 7.28 MGOe for the FePt–FeCo particles with 0.9 ± 0.279 nm thick FeCo shells, indicating the effective ESC at the interface between the hard and soft phases. This energy product value decreased for thicker FeCo shells, but was much larger than that of pure FePt when the FeCo shell thickness was less than 1.2 nm (5.1 MGOe). This indicated that the energy product could be maximized such that the H_c could continue to grow and maintain a sufficiently high M_s. As the FeCo shell thickness was further increased, the M_s value could not compensate for the drop in H_c, leading to a decrease in the $(BH)_{max}$ value. Therefore, the magnetic energy product performance was determined by the thickness of the FeCo shell. Furthermore, the B–H curves of the samples with the thinnest shells (0.9 ± 0.279 nm) were also investigated at different sintering temperatures. The inset of Fig. 4b displays

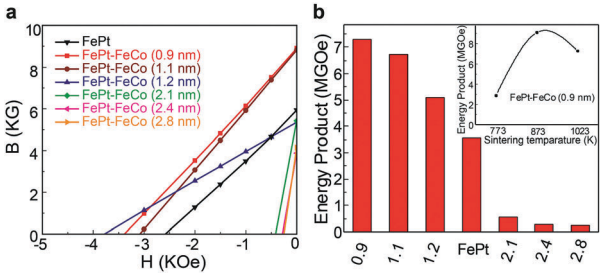

Fig. 4 Energy product of FePt–FeCo nanoparticles. (a) Second-quadrant B–H curves for FePt–FeCo nanoparticles annealed at 1023 K for 2 h with different shell thicknesses. (b) Calculated energy products of samples shown in (a), with the inset showing the calculated energy products for FePt–FeCo with shell thicknesses of 0.9 nm after sintering at different temperatures for 2 h.

the energy products of samples sintered at 773 K, 873 K, and 1023 K. The 873 K sintered sample exhibited an optimum energy product of 9.11 MGOe. This was attributed to FeCo shell diffusion at a higher sintering temperature of 1023 K, which led to saturation magnetization loss and minor separation between the two magnetic phases.

Ultimately, a solution-based nano-synthesis method was developed by coating a magnetically soft FeCo shell onto a hard FePt core to produce core–shell nanostructures with controlled shell thicknesses. The exchange coupling and enhanced spin canting effects were realized by controlling the FeCo shell thickness, leading to enhanced coercivities and increased energy products in FePt–FeCo nanostructures. The spin canting techniques provided new opportunities for designing high performance magnetic core–shell nanostructures.

S. R. acknowledges the support from the U.S. National Science Foundation (NSF) under the CAREER Award No: NSF-DMR-1830749. A. X. G. acknowledges support from the U.S. Army Research Office, under Grant No. W911NF-15-1-0181. Work at the Molecular Foundry was supported by the Office of Science, Office of Basic Energy Sciences, of the U.S. Department of Energy under Contract No. DE-AC02-05CH11231. Research reported in this document was supported in part under contract W911-QX-16-D-0014 by SURVICE Engineering and under contract W911NF-16-2-0050 by the Oak Ridge Institute for Science and Education through an interagency agreement between the U.S. Department of Energy and the U.S. Army Research Laboratory. The views and conclusions contained in this document are those of the authors and should not be interpreted as representing the official policies, either expressed or implied, of the Army Research Laboratory or the U.S. Government. The U.S. Government is authorized to reproduce and distribute reprints for Government purposes not withstanding any copyright notation herein.

Conflicts of interest

There are no conflicts to declare.

Notes and references

1 A. H. Lu, E. e. L. Salabas and F. Schüth, *Angew. Chem., Int. Ed.*, 2007, **46**(8), 1222–1244.
2 X. Liu, S. He, J.-M. Qiu and J.-P. Wang, *Appl. Phys. Lett.*, 2011, **98**(22), 222507.
3 N. De Sousa, A. Apolinario, F. Vernay, P. Monteiro, F. Albertini, F. Casoli, H. Kachkachi and D. Schmool, *Phys. Rev. B: Condens. Matter Mater. Phys.*, 2010, **82**(10), 104433.
4 U. Kawald, W. Zemke, H. Bach, J. Pelzl and G. Saunders, *Phys. B*, 1990, **161**(1–3), 72–74.
5 D. J. Carnevale, M. Shatruk and G. F. Strouse, *Chem. Mater.*, 2016, **28**(15), 5480–5487.
6 J. H. Lee, J. T. Jang, J. S. Choi, S. H. Moon, S. H. Noh, J. W. Kim, J. G. Kim, I. S. Kim, K. I. Park and J. Cheon, *Nat. Nanotechnol.*, 2011, **6**(7), 418.
7 F. Liu, J. Zhu, W. Yang, Y. Dong, Y. Hou, C. Zhang, H. Yin and S. Sun, *Angew. Chem.*, 2014, **126**(8), 2208–2212.
8 D. J. Carnevale, M. Shatruk and G. F. Strouse, *Chem. Mater.*, 2016, **28**(15), 5480–5487.
9 C. Yang, L. Jia, S. Wang, C. Gao, D. Shi, Y. Hou and S. S. Gao, *Sci. Rep.*, 2013, **3**, 3542.
10 E. F. Kneller and R. Hawig, *IEEE Trans. Magn.*, 1991, **27**(4), 3588–3600.
11 F. Liu, Y. Hou and S. Gao, *Chem. Soc. Rev.*, 2014, **43**(23), 8098–8113.
12 Q. Song and Z. J. Zhang, *J. Am. Chem. Soc.*, 2012, **134**(24), 10182–10190.
13 H. Zeng, J. Li, J. P. Liu, Z. L. Wang and S. Sun, *Nature*, 2002, **420**(6914), 395–398.
14 W. Zhang, K. Patel and S. Ren, *Nanoscale*, 2017, **9**(35), 13203–13208.
15 C. Xu, K. Xu, H. Gu, R. Zheng, H. Liu, X. Zhang, Z. Guo and B. Xu, *J. Am. Chem. Soc.*, 2004, **126**(32), 9938–9939.
16 J. Gao, H. Gu and B. Xu, *Acc. Chem. Res.*, 2009, **42**(8), 1097–1107.
17 S. H. Moon, S.-H. Noh, J.-H. Lee, T.-H. Shin, Y. Lim and J. Cheon, *Nano Lett.*, 2017, **17**(2), 800–804.
18 C. Wang, Y. Hou, J. Kim and S. Sun, *Angew. Chem.*, 2007, **119**(33), 6449–6451.
19 W. Chen, J. Kim, S. Sun and S. Chen, *Langmuir*, 2007, **23**(22), 11303–11310.
20 T. Klemmer, N. Shukla, C. Liu, X. Wu, E. Svedberg, O. Mryasov, R. Chantrell, D. Weller, M. Tanase and D. Laughlin, *Appl. Phys. Lett.*, 2002, **81**(12), 2220–2222.
21 M. Müller and K. Albe, *Phys. Rev. B: Condens. Matter Mater. Phys.*, 2005, **72**(9), 094203.
22 J. Kim, C. Rong, J. P. Liu and S. Sun, *Adv. Mater.*, 2009, **21**(8), 906–909.
23 B. Chen, K. Lutker, S. V. Raju, J. Yan, W. Kanitpanyacharoen, J. Lei, S. Yang, H.-R. Wenk, H.-K. Mao and Q. Williams, *Science*, 2012, **338**(6113), 1448–1451.
24 V. Petkov and S. D. Shastri, *Phys. Rev. B: Condens. Matter Mater. Phys.*, 2010, **81**(16), 165428.
25 R. Medwal, N. Sehdev and S. Annapoorni, *J. Phys. D: Appl. Phys.*, 2012, **45**(5), 055001.
26 O. Gutfleisch, J. Lyubina, K. H. Müller and L. Schultz, *Adv. Eng. Mater.*, 2005, **7**(4), 208–212.
27 T. Tanaka, J. Matsuzaki, H. Kurisu and S. Yamamoto, *J. Magn. Magn. Mater.*, 2008, **320**(22), 3100–3103.

